



HAL
open science

SUMMER DIURNAL CYCLE AT DOME C ON THE ANTARTIC PLATEAU

Hélène Barral, E Vignon, E Bazile, O Traullé, Hubert Gallée, Christophe
Genthon, Christophe Brun, F Couvreur, P Le Moigne

► **To cite this version:**

Hélène Barral, E Vignon, E Bazile, O Traullé, Hubert Gallée, et al.. SUMMER DIURNAL CYCLE AT DOME C ON THE ANTARTIC PLATEAU. 21st Symposium on Boundary Layer and Turbulence, AMS, Jun 2014, Leeds, United Kingdom. hal-01140962

HAL Id: hal-01140962

<https://hal.univ-grenoble-alpes.fr/hal-01140962>

Submitted on 10 Apr 2015

HAL is a multi-disciplinary open access archive for the deposit and dissemination of scientific research documents, whether they are published or not. The documents may come from teaching and research institutions in France or abroad, or from public or private research centers.

L'archive ouverte pluridisciplinaire **HAL**, est destinée au dépôt et à la diffusion de documents scientifiques de niveau recherche, publiés ou non, émanant des établissements d'enseignement et de recherche français ou étrangers, des laboratoires publics ou privés.

SUMMER DIURNAL CYCLE AT DOME C ON THE ANTARTIC PLATEAU

H. Barral^{1,3*}, E. Vignon¹, E. Bazile⁴, O. Traullé⁴, H. Gallée¹, C. Genthon¹, C. Brun³, F. Couvreur⁴, P. Le Moigne⁴

¹CNRS, LGGE, (UMR5183), F-38000 Grenoble, France

²Univ. Grenoble Alpes, LGGE, (UMR5183), F-38000 Grenoble, France

³Univ. Grenoble Alpes, LEGI, (UMR5519), F-38000 Grenoble, France

⁴CNRM, Météo-France, Toulouse, France

1 INTRODUCTION

Antarctic boundary layers experience persistent and strong temperature inversions (*Phillpot and Zillman, 1970; King and Turner, 1997*). A better understanding of the physical processes and their coupling involved in stable boundary layers is necessary to model the Antarctic meteorology and for future predictions of the regional climate and sea level. The study of the Antarctic atmosphere may also help to investigate the stable boundary layers. Indeed, the ice-sheet offers us "laboratory cases" with endless snow covered, relatively homogeneous, flat or sloped areas with persistent and strong stable stratifications resulting in low level jets. Dome C (75°06 S, 123°E) on the East Antarctic Plateau is one of them.

Dome C is a place of particular interest partly because of the numerous observations performed there, all year long. The nearby permanent scientific station Concordia, jointly operated by the French and Italian polar institutes (IPEV and PNRA) allows routinely operating permanent observations despite the remoteness of the site, the very low temperatures and the frost deposition.

Figure 1 shows the topography of the dome culminating at 3233 m above sea level; the local slope is no greater than 1‰ so that the place does not feed the famous strong and persistent katabatic winds of Antarctica (*Parish and Bromwich, 2007*). No clear annual cycle in wind speed has been noticed, the annual speed averages 4.5 ms^{-1} at 10 m according to

*. Corresponding author : H el ene Barral, Laboratoire de Glaciologie et de G eophysique de l'Environnement, BP96, F-38400 Grenoble helene.barral@lgge.obs.ujf-grenoble.fr

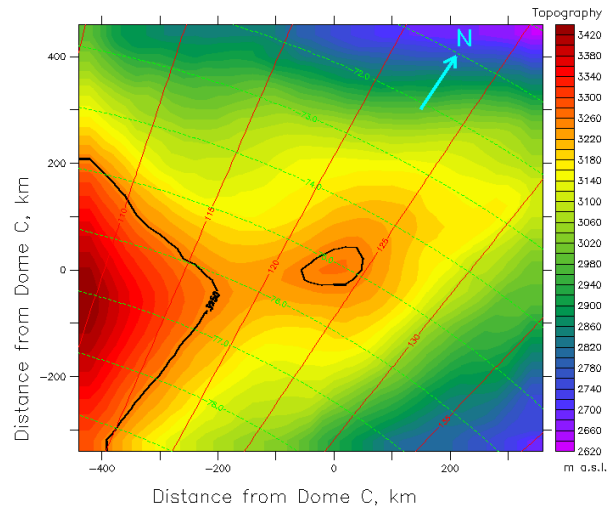


FIGURE 1 – Topography around Dome C - (*Gall e et al., 2014a*)

tower observations.

In summer, this high latitude area is permanently insolated, still the boundary layer experiences a clear diurnal cycle in temperature and wind speed. This summertime boundary layer has been investigated through several measurement methods : in-situ meteorological sensors (*Genthon et al., 2010, 2013*), ground-based sodar (*Argentini et al., 2005, 2014*), and ground-based microwave radiometer (*Ricaud et al., 2011*). At "night" that is when the sun zenith angle is the largest, the albedo of the surface is also the highest (around 0.85), the net long-wave deficit $LW \uparrow - LW \downarrow$ exceeds the net short-wave gain $SW \downarrow - SW \uparrow$ leading to surface cooling. Clear sky and weak wind conditions favour the development of a strongly stably stratified boundary layer. During

the day, high downward solar radiative fluxes and dryness associated to low temperatures ($\sim -30^\circ\text{C}$) favour the initiation of convection (*King et al.*, 2006). A well mixed layer grows up to 200 or 300 m above the surface (*Argentini et al.*, 2005, 2014; *Ricaud et al.*, 2011). Such a diurnal cycle, with a boundary layer experiencing such a broad range of turbulence regime is not common even in Antarctica, the land of uncommons.

King et al. (2006) compare the diurnal responses of the boundary layer of Halley and Dome C, both around 75°S . At Halley which surface receives approximately the same amount of daily radiation, the measured diurnal temperature amplitude (at 2 m) typically reaches 3°C compared to 10°C at Dome C. The difference is attributed to 1) a lower daytime heating due to different partitioning of available surface energy into fluxes of latent or sensible heat ; 2) a lower night-time cooling due to difference in cloud cover. *King et al.* (2006) conclude that in order to experience a summertime convective boundary layer in Antarctica, one should be northerly enough for sufficient daytime solar radiation and also elevated enough for low temperatures (so that the energy absorbed by the surface is transferred to the boundary layer through sensible rather than latent heat, and thus is able to initiate convection). However, on the ice-sheet altitude is roughly correlated with latitude. Moreover, going northward, cloud cover and mechanical mixing due to katabatic wind prevent the formation of a strongly stably stratified boundary layer. Dome C appears to be a good synergy between latitude and altitude.

Low level jets are commonly observed in stable boundary layers. They may be downslope flows (*Manins and Sawford*, 1979) or "short-lived" jet, induced by an inertial oscillation during the "evening transition" (*van de Wiel et al.*, 2010). This study focuses on a particular diurnal cycle : the 11th and 12th December 2009. Single column model simulations are performed and compared to in-situ observations. Then we focus on night-time turbulent mixing and search for possible underlying mechanisms for a nocturnal low level jet.

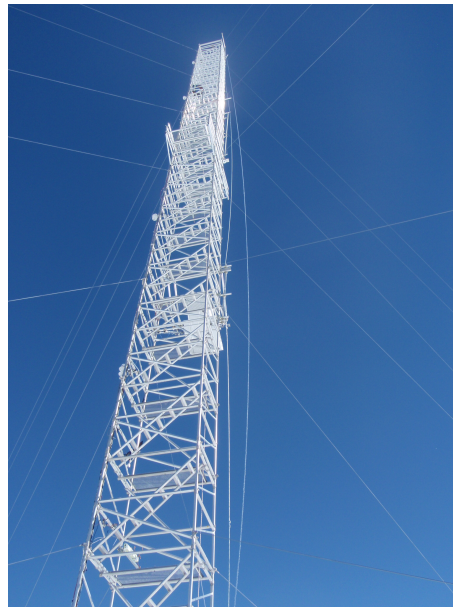


FIGURE 2 – The 45 m tower at Dome C (Photo C. Brun)

2 OBSERVATIONS and MODELLING TOOLS

2.1 Observations system : the 45-m tower

Several kinds of atmospheric and snow pack observations are routinely performed at Dome C. In particular six level of meteorological sensors have been set up from 3 to 42 m on the tower depicted in Figure 2.

Wind speed and direction are measured with Young 05103 aerovanes, air temperature and relative humidity are sampled with Vaisala HMP155, in aspirated shields. Up to now, a 5-year quasi-continuous data series has been recorded. *Genthon et al.* (2010, 2011, 2013) give further details on this tower measurements, the obtained mean statistics and the deduced main characteristics of the boundary layer. In addition to these "standard" meteorological sensors, six sonic thermo-anemometers were deployed between 7 and 42 m. In December 2009, five of them were running.

Everyday, insights of the state of the atmosphere up to 20-25 km over Dome C are provided by launching Vaisala RS92 radiosound around 12 UTC (20 LT) as part as the Rou-

tine Meteorological Observation program[†]. In December 2009, during the Concordiasi campaign detailed by *Rabier et al.* (2010), an additional radiosound was launched around 0 UTC (8LT).

2.2 The Meso-NH numerical model

Meso-NH is a non-hydrostatic, anelastic model designed to simulate a broad range of atmospheric motions from mesoscale to turbulent eddies (*Lafore et al.*, 1998). Here, it was used in single column mode coupled with the SURFEX surface scheme (*Masson et al.*, 2013). A 1.5-order turbulent scheme as described in *Cuxart et al.* (2000), based on a prognostic equation for TKE and involving a Richardson-number-dependent formulation for the Prandtl number (*Redelsperger and Sommeria*, 1982) is implemented. It is used here in its one dimensional formulation with a *Bougeault and Lacarrère* (1989) mixing length. The long-waves and short-waves radiative transfers are computed separately using the ECMWF operational radiation code (*Gregory et al.*, 2000). Cloud dynamics is simulated using a mixed-phase microphysical scheme (*Pinty and Jabouille*, 1998); shallow convection is parameterized with a combined eddy-diffusivity / mass-flux approach (*Pergaud et al.*, 2009).

2.3 Initialization and large-scale forcing

The case starts at 0 UTC that is 8LT in the morning. A radiosounding is available at that time. Actually, this observational data are not directly used. Instead, temperature, humidity and geostrophic wind initial fields have been deduced and simplified (*Bazile et al.*, 2014) from a 4D-var re-analysis with the ARPEGE global circulation model. The re-analysis was performed using the ARPEGE configurations used during the Concordiasi field campaign : a stretched grid centred on Dome C with horizontal resolution of 10 km on the Antarctic plateau. Each radiosounding of the period was taken into account with its whole set of data levels.

[†]. RMO, <http://www.climantartide.it/>.

For meaningful comparison between simulations and observations, we must prescribe a realistic large scale atmospheric forcing corresponding to the studied period. The needed large-scale fields are the geostrophic wind and the dynamical tendencies of temperature and humidity induced by the synoptic-scale weather conditions. These fields and their temporal evolutions are not observed but deduced by comparison of modelling and radiosounding data (*Bazile et al.*, 2013). An ensemble of simulations with the three dimensional limited area model AROME (*Seity et al.*, 2010) forced by the ARPEGE reanalysis and coupled with different physical packages were performed.

The AROME horizontal pressure gradient is used as an estimator of the geostrophic wind. The dynamic contributions to tendencies $\frac{\partial T}{\partial t}$ and $\frac{\partial q}{\partial t}$ were isolated by subtracting the mean spatially averaged physical tendencies only obtained with the AROME ensemble simulations from the tendencies observed between two consecutive radiosounding measurements.

Four profiles for +0 h, +12 h, +24 h and +36 h have been designed. In between, the model computes a linear interpolation of the two consecutive forcings. The advection tendencies of temperature and humidity are kept constant in each 12 h period. These initial and forcing fields were preliminary in-test versions of the GABLS4 intercomparison project (*Bazile et al.*, 2014).

2.4 Model setup

A reference simulation was performed with 10 m resolution in the low troposphere and a first level at 5 m. The stretched vertical grid extends up to 9000 m above the surface, with a damping layer above 8 km. The time step is set to 30 s. Microphysics, radiation, turbulence, shallow convection and surface schemes are activated. The chosen surface scheme consists in a 3 layers soil with the surface characteristics of fresh snow. The following surface parameters are fixed and do not evolve : the albedo ($\alpha = 0.8$), the surface roughness ($z_0 = 0.01$ m) and the emissivity ($\epsilon = 0.98$). The simulation starts on 11 December at 00 UTC (8LT) and runs 36 hours.

3 THE DIURNAL CYCLE on DECEMBER 11-12th, 2009.

3.1 Comparison with December climatology

To assess whether the study period (11 and 12 December 2009) is representative of the summertime at Dome C, observed data from five December months (2009 to 2013) have been gathered and compared to the data collected during the study period (*Vignon, 2014*). For a saturated air parcel at -30°C and 650 hPa , specific humidity is of about $0.35\text{ g}\cdot\text{kg}^{-1}$. This is a very low value : the atmosphere may be considered as dry. Consequently, the present study does not discuss moisture aspects of the boundary layer but focuses on the temperature and wind climatology. In fact, no moisture climatology has been drawn due to the lack of accurate humidity measurements. In such dry conditions, standard humidity measurements are questionable (*Genthon et al., 2013*).

3.1.1 December climatology

Located 1000km away from the Coast, cloud cover is relatively thin or absent (*King and Turner, 1997*). For the last 5 summers the measured $LW\downarrow$ flux is under 125 Wm^{-2} more than 75 % of the time (Figure 3).

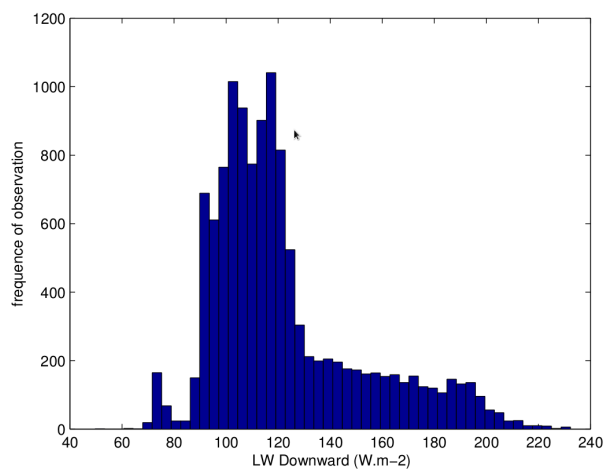


FIGURE 3 – Histogram - longwave diffusive radiation down : $LW\downarrow$. BSRN data, December only from 2009 to 2013 - (*Vignon, 2014*).

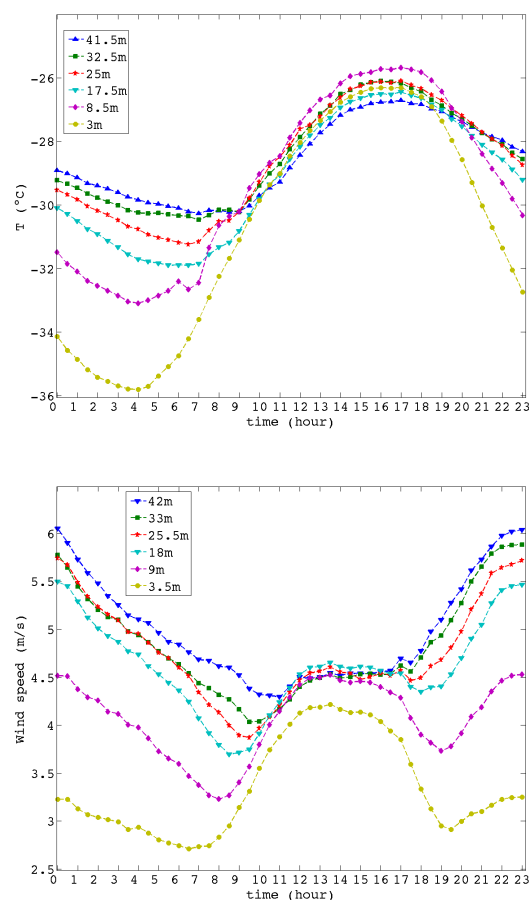


FIGURE 4 – Mean diurnal cycle in temperature and wind speed. Night-time December data from 2009 to 2011.

Temperature. Temperature usually averages around -30°C in summer but experiences diurnal variations with an amplitude of about 10°C at 3 m, damping to 4°C at 42 m as shown in Figure 4.

Daytime profiles are quasi-uniform along the tower. This turbulent mixed layer fed by convection deepens from about 20-30 m at 9 am up to 100-300 m, as estimated by sodar measurements (*Argentini et al.*, 2005, 2014). From 4-5 pm, as soon as the heat turbulent fluxes decrease below zero, the mixed layer collapses to 50 m within only 2 hours. A stable stratification starts to set up in the surface layer.

Observed night-time temperature profiles obtained from the tower and radiosoundings may be divided in three layers. The inversion layer extends in the lowest 20 meters. The inversion layer characterised by a temperature gradient of $0.7^{\circ}\text{C} \cdot \text{m}^{-1}$ thickens regularly from 8 pm to 7 am, before shrinking suddenly. An overlying residual layer, with uniform temperature follows and overpasses the top of the tower. Above and up to the tropopause, the atmosphere is weakly stable with a quasi-uniform gradient, and a Brunt Väisälä frequency about $N \sim 0.014\text{s}^{-1}$. The maximum daytime temperature is reached 1 hour after midday for the surface temperature, 2 hours later (3 pm) at 3 m and around 4-4.5 pm at 40 m above the surface. The minimum night-time temperature is reached at about 2 am for the surface temperature, 2 hours later (4 am) at 3 m and at about 6 am at 25 m above the surface.

Wind. More than 80 % of the time, wind blows from South, South-West, bringing dry and cold air from the high plateau (Figure 5). Northerly winds occur sometimes and are correlated with so-called warm events (*Genthon et al.*, 2010). Daytime vertical wind profiles are quasi-homogeneous in the mixed layer. Conversely, night-time wind profiles are characterized by a strong wind shear $\frac{dW}{dz} \sim 0.075\text{s}^{-1}$. The near surface wind, weaker by night, plateaus at 4.5ms^{-1} by day, while active turbulent mixing may bring momentum from the upper troposphere. On the tower top, the midday plateau consists in a minimum, the maximum is reached by night.

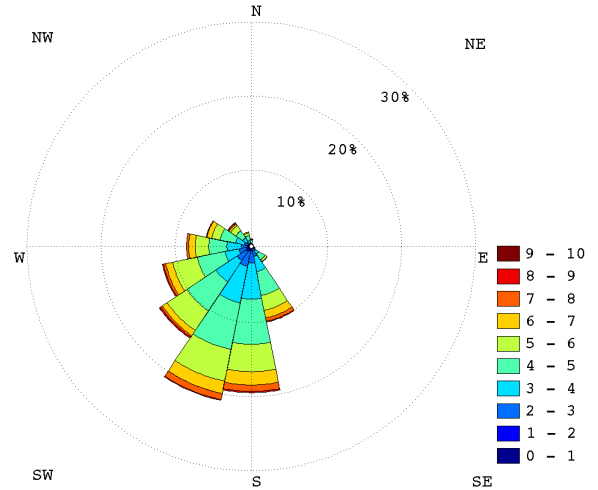


FIGURE 5 – Wind rose - 9-m wind, December (only) data from 2009 to 2011

3.1.2 December 11-12th, 2009

Temperature and velocity profiles in the boundary layer are typical of a summer day. In the lowest 15 m, the temperature is a bit colder than the climatological mean as other clear sky days. $LW \downarrow$ varies between 90 and 100Wm^{-2} . Wind is South-Westerly. Along the tower it is slightly weaker ($\sim 1\text{ms}^{-1}$) than the climatological mean but still in the \pm one standard deviation interval. Figure 6 shows that the near-surface stratification in the early morning is one of the strongest observed ($T_{3.3\text{m}} - T_s > 10\text{K}$), as expected for clear-sky and weak wind conditions.

3.2 Diurnal cycle in temperature

Isocontours of the observed and simulated potential temperature profiles are presented in Figure 8. The simulated temperature field experiences a clear diurnal cycle in phase with the observed cycle. Neither the surface temperature nor the fluxes are prescribed, so that, the cycle expresses the response of the boundary layer to solar forcing. The simulated boundary layer is stably stratified at night (with a temperature gradient reaching 0.11Km^{-1} between 3 and 60 m) and relatively well mixed during the day. Evening and morning transitions seem on the whole well reproduced and occur in time.

However, the vertical distribution of temperature is not satisfactory. In order to be com-

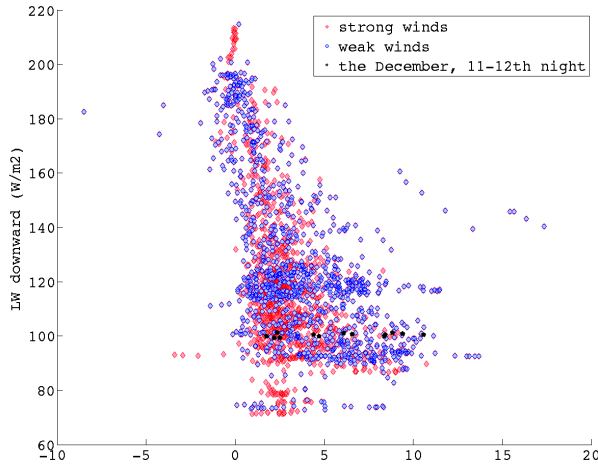


FIGURE 6 – Downward long-waves radiation $LW \downarrow$ versus Inversion strength in the surface layer ($T_{3.3m} - T_s$), by night. Strong winds samples are plotted in red, whereas weak winds samples in blue. Plotted samples are from night-time December (only) data from 2009 to 2013. - Adapted from (Vignon, 2014).

parable, simulated and observed temperature profiles are shown in Figure 8 using two different vertical scales. The simulated temperature field is plotted up to 180 m above the surface, whereas observed temperatures are plotted only along the 45 m of the tower. The simulated inversion layer follows similar thickening and shrinking phases than the observed one but extends up to 60 m. In addition, there is no clear residual layer above.

The order of magnitude of the daytime near-surface temperature is well reproduced with a temperature maximum around -27.5°C ($\theta \sim 278\text{K}$). But, the surface layer does not cool enough at night, leading to a warm bias in the simulation. The near surface diurnal amplitude is thus underestimated, scaling around 10°C at the surface and 9°C at 3 m whereas, in the observational data, the diurnal amplitude reaches 17°C at the surface and 12°C at 3 m. The amplitude is damped to 8°C at 20 m; the simulated damping is underestimated and only reaches 1°C , consistent with a too deep inversion layer.

3.3 Diurnal cycle in wind speed

The simulated 3.5 m mean wind speed is quite close to the observed one ($\sim 2.5\text{ms}^{-1}$), however, the 10 m mean wind speed is un-

derestimated by about 0.25ms^{-1} . Figure 9 shows the velocity profile (1 h averaged) during the whole simulation. During the "day" (between 11 am et 4 pm) the velocity vertical profile is uniform along the tower. Whereas, at "night", a strong shear is observed in the first 20 meters. Despite an overestimation of daytime shear and an underestimation of nighttime shear, the diurnal cycle in wind speed is in overall well reproduced by the model.

Figure 10 exhibits the wind speed isocontours as observed (top) and simulated (bottom). Two velocity maxima can be seen by night. From tower observations, a first maximum is visible at 10 pm with a 6.1ms^{-1} speed. The maximum speed is measured by the highest anemometer, we suppose this is the signature of a jet since the speed exceeds the geostrophic speed as estimated by AROME (section 2.3, and used to force the model). Nevertheless, we do not know exactly the jet nose position. It could be higher, or a bit lower since the difference in the two speed measured from the two highest anemometers is far lower than the factory stated accuracy ($\Delta W \sim \pm 0.03\text{ms}^{-1} < \sigma_W = 0.3\text{ms}^{-1}$). The jet nose looks going down below 10 m at 2 h30. Around 9 am, a second maximum is measured at the top.

The model also produces two distinct wind speed maxima. A jet is simulated around 1 am with a nose located at 58 m and a speed of 7.1ms^{-1} . The speed exceeds the geostrophic wind speed G by 2.3ms^{-1} . A second supergeostrophic maximum of $6.5\text{ms}^{-1} = G + 1.3\text{ms}^{-1}$ is reached at about 9 am and is located near 200 m. Figure 11 compares the temporal series of observed and simulated wind speed. Despite the too high location of the wind maxima, the timing is quite satisfactory.

In the simulation, the geostrophic wind is forced and evolves in time. However, from 0 to 400 m the geostrophic wind speed is vertically uniform and varies only slightly temporally, $G = 4.7\text{ms}^{-1}$ with a standard deviation of 0.33ms^{-1} . Nevertheless, in order to be sure that the maximum speed described here is not correlated with temporal extrema in geostrophic wind, a simulation with a constant geostrophic forcing has been performed. The results reported in Table 1 do

not significantly change. Two supergeostrophic maxima are again simulated. The wind maxima are weaker consistent with a weaker geostrophic wind, $W_{J1} = G + 2.1 \text{ ms}^{-1}$, $W_{J2} = G + 1.7 \text{ ms}^{-1}$. A dynamical explanation of the wind maxima as low level jet is sketched in section 5.

4 TURBULENT MIXING

The model performs quite well during the day but fails in reproducing the stable stratification at night (section 3.2). Possible reasons could be an unrealistic turbulent mixing or a misrepresentation of snow-surface processes. This section investigates the first scenario and focuses on night-time turbulent mixing. First the simulation is compared to turbulent quantities deduced from in-situ observations. Then, the turbulent scheme of the Meso-NH model is analyzed.

Figure 12 shows normalised vertical profiles of potential temperature, wind speed and TKE at midnight. Figure 13 shows the contributions of different terms in the TKE budget equations. Turbulent kinetic energy is mainly produced by shear in the 60 lowest meters. The top of the turbulent layer corresponds to the top of the inversion layer and to the height of the jet. Studying a case of nocturnal low level jets in the Duero Basin, Spain, *Conangla and Cuxart* (2006) and *Cuxart and Jiménez* (2007) have found with Meso-NH simulations two distinct turbulent layers. Vertical profiles of TKE is maximum near the surface and above the jet nose due to shear production. These two layers of elevated turbulence are separated by a minimum around the jet nose. The two-layer structure is not simulated here (Figure 13). Maybe this is because our jet is less pronounced and "short lived". The jet studied by *Cuxart and Jiménez* (2007) is quasi-stationary between 0000 and 0200 UTC with values around 9 ms^{-1} .

Turbulent quantities as turbulent kinetic energy, heat and momentum fluxes and temperature variances have been computed from sonic-anemometers data and eddy correlation (EC) methods. Surface fluxes have been computed through profile method

from classical meteorological measurements and similarity laws (*Vignon*, 2014). Some of these quantities are compared here to the simulated one (Figure 14).

Surface sensible heat flux is in a good agreement with observations whereas the surface friction velocity is significantly overestimated (by 40 %) (not shown). Correct values of surface sensible heat fluxes are not expected since snow-surface temperature does not cool enough at night leading to a warm bias of about 6 K. Changing the roughness length to a more realistic value $z_{0\text{Simu2}} = 0.001 \text{ m}$ instead of $z_{0\text{Simu1}} = 0.01 \text{ m}$ leads to a lower surface friction velocity, which is still overestimated, but by 30 %. The surface sensible heat flux is improved whereas TKE at 7 m deteriorates (not show). Overall the simulated boundary layer is slightly more stable and thinner (Table 1), but improvements are limited.

Figure 14 compares temporal series of turbulent quantities at 7 meters computed by the Meso-NH model and by eddy correlation methods. The height of 7 m falls between the first and second model atmospheric levels (3.7 m and 11.2 m). Turbulent kinetic energy (e), potential temperature variance ($\overline{\theta'^2}$), sensible heat ($\overline{w'\theta'}$) and momentum fluxes ($\overline{w'u'}$) are shown in Figure 14. Simulated and observed diurnal trends are similar, whereas their order of magnitude differs. At 7 m above the surface, while values of TKE (e) are comparable, and $\overline{\theta'^2}$ is overestimated, $\overline{w'\theta'}$, $\overline{w'u'}$ and $\overline{w'v'}$ are overestimated by Meso-NH. As one goes upper, for example at 30 m, the agreement tends to be better (not shown). This overestimation of turbulent mixing intensity in the inversion layer may explain the difficulty of the model to represent the observed strength of the stable stratification and its shallowness.

In fact, misrepresentation of the second order moments : $\overline{\theta'^2}$, $\overline{w'\theta'}$, $\overline{w'u'}$ and $\overline{w'v'}$, by night is expected since vertical gradients of potential temperature θ and, to a lesser extent, of wind speed are largely underestimated by the model. The model turbulent-scheme computes

	z_0 m	G ms ⁻¹	$\frac{dT}{dz})_{J1}$ Km ⁻¹	First wind maximum			Second wind maximum		
				t_{J1} LT	z_{J1} m	W_{J1} ms ⁻¹	t_{J2} LT	z_{J2} m	W_{J2} ms ⁻¹
Simu1 Ref	0.01	4.7 ± 0.5	0.115	1 ± 1	58	7.11	9 ± 1	210	6.54
Simu2 z_0	0.001	4.7 ± 0.5	0.12	1 ± 1	50	6.82	9 ± 1	195	6.34
Simu3 $G = cst$	0.01	4.4 ± 0.0	0.11	0 ± 1	50	6.45	10 ± 1	125	6.06
Obs			0.3	22	33	6.03	10 ± 0.5	> 42	

TABLE 1 – Time, height and strength of the simulated and observed jets. Three different simulations are compared, the control simulation (Ref), one with a lower rugosity length (Simu2) and another with constant geostrophic forcing (Simu3).

the second order moments using a K -gradient approach.

Figure 15 shows the vertical profile of the eddy diffusivity coefficient K_h for sensible heat at midnight. The simulated K_h decreases with height. The eddy-diffusivity coefficient deduced from eddy correlation appears quite noisy in this instantaneous picture, but the lowest value at 7 m is relatively constant along the night. At 7 m $(K_h)_{\text{obs}} \sim 0.005 \text{ m}^2 \text{ s}^{-1}$ whereas $(K_h)_{\text{simu}} \sim 0.1 \text{ m}^2 \text{ s}^{-1}$. $(K_h)_{\text{simu}}$ is computed by the Meso-NH closure scheme according to, (*Cuxart et al.*, 2000) :

$$K_h = C_h \cdot l \cdot \sqrt{e} \cdot \phi \quad (1)$$

where e denotes the turbulent kinetic energy. l is the *Bougeault and Lacarrère* (1989) mixing length representing the size of the most energetic subgrid eddies. ϕ is a stability function, it accounts for the Prandtl number dependence on Richardson number, and $C_h = 0.14$ is a fixed parameter. In one-dimensional cases, ϕ gets a simple formulation, (*Cuxart et al.*, 2000) :

$$\phi(z) = \frac{1}{1 + C_1 \beta \frac{l^2}{e} \frac{\partial \bar{\theta}}{\partial z}} \quad (2)$$

with $C_1 = 0.0257$. β denotes the buoyant parameter $\beta = \frac{g}{\theta_r}$, and $\frac{\partial \bar{\theta}}{\partial z}$ is the local vertical gradient of temperature.

In a layer of constant stable stratification $\frac{\partial \bar{\theta}}{\partial z}$, a simple analytical formulation for l can be obtained from a second order development of $\theta(z) - \theta(z')$, (*Bougeault and Lacarrère*, 1989) :

$$l = \sqrt{\frac{2e}{\beta \frac{\partial \bar{\theta}}{\partial z}}} \quad (3)$$

Combining equations (3) and (2) in equation (1), K_h becomes :

$$K_h \sim C_h \frac{\sqrt{2}}{1 + 2C_1} \frac{e}{\sqrt{\beta \frac{\partial \bar{\theta}}{\partial z}}} \quad (4)$$

The equation implies that K_h is a decreasing function of the stratification parameter $\frac{\partial \bar{\theta}}{\partial z}$. Figure 16 shows the shape of K_h as a function of $\frac{\partial \bar{\theta}}{\partial z}$ for different values of e .

Computing K_h from equation (4) with modeled values of $\frac{\partial \bar{\theta}}{\partial z}$ and e , it gives : $(K_h)_{\text{analytic1}} \sim 0.13 \text{ m}^2 \text{ s}^{-1}$. This is larger than $(K_h)_{\text{simu}} \sim 0.10 \text{ m}^2 \text{ s}^{-1}$. However it is the right order of magnitude, and is far larger than the value deduced from observations : $(K_h)_{\text{obs}} \sim 0.001 \text{ m}^2 \text{ s}^{-1}$. Suppose that the simulation performs better in reproducing the stable stratification so that at midnight the simulated vertical gradient of temperature approaches the observed one. Then, according to equation (4) : $(K_h)_{\text{analytic2}} = 0.06 \text{ m}^2 \text{ s}^{-1}$, this value is lower but still one order of magnitude too large.

The values of vertical gradient of temperature and turbulent kinetic energy, at midnight, 7 m above the surface are reported in Table 2. The corresponding observed or computed eddy-diffusivity coefficients K_h and fluxes $\overline{w'\theta'}$ are reported in the same table and in Figure 16. The analytic study detailed in the case of sensible heat flux and summarized in Figure 16 shows that the model overestimates turbulent mixing. Even though the stable stratification was well reproduced, it could not be sustained due to a too large mixing length l or a too large coefficient C_h . A

simulation initialized with the observed temperature profile at 2am instead of 8am has been performed. It did not give better results : the steep initial temperature gradient is rapidly smoothed, supporting the conclusion drawn from the analytic study. Dividing C_h by 30 in equation (1) would resolved the problem at the beginning of the night, but it may alter good results during day time. The adjustment of the parameter C_h is part of ongoing work.

5 THE LOW LEVEL JET

5.1 Climatological study

Both in the observations and simulations, the two low level jets occur at the top of the inversion layer. The simulated jet is too high compared with the observed one but this is consistent with the weaker stability and deeper inversion layer. This kind of nocturnal jet is not specific to our case study as a jet is observed below 41 m (the highest anemometer) more than 90% of the 5 last years December nights (*Vignon, 2014*). Figure 4 shows that contrary to the near-surface wind, the 20 to 40-m winds reach their maximum by night. This averaged maximum speed is probably associated to a low level jet. Climatological wind standard deviation increases with height by night (reaching 1.5 ms^{-1}), so that the clear maximum wind speed seen in Figure 4 at midnight, hides disparities in the low level jet nose and maximum. The jet characteristics vary from day to day probably depending on inversion strength and on geostrophic wind. Inversion strength itself depends on external forcing like cloud cover. Figure 7 shows the height of the jet nose is lower when the inversion is stronger.

Inversion related low level jets are usually associated to katabatic flows. The surface is flat at Dome C, so that katabatic flows can not be locally generated. However, map 1 shows a 300 km-long slope, down from the South-Western high plateau to a pass 200 m lower. The slope direction corroborates with the prevailing wind. From the pass the terrain height increases by 40 m over 100 km and reaches Dome C. Nocturnal radiative cooling during

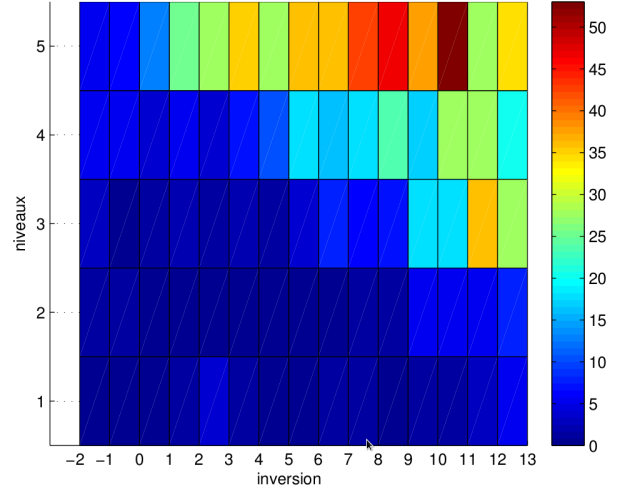


FIGURE 7 – Number of samples (30-min average) for which a jet is detected below 40 m, depending on the height (expressed in tower level) and the inversion strength (measured by $T_{\text{tower top}} - T_{\text{tower bottom}}$ in $^{\circ}\text{C}$). All the available measurements recorded during December nights from 2009 to 2013 have been plotted. - Adapted from (*Vignon, 2014*).

the short 'night' very probably induces katabatic flows on these two slopes. Could one consider that katabatic flows generated on the down-slope to have enough kinetic energy to reach Dome C?

Gallée et al. (2014b) have studied an other case of low level jet at Dome C on December 16-17th, 2011. The limited area model, specially designed for Antarctic meteorology MAR, nudged with ECMWF reanalysis fields is used. The simulation is made on the 3-D domain represented in Figure 1. Height and speed of the nocturnal low level jet are remarkably simulated. An analysis of the simulation on that case shows that katabatic winds flow down-slope but do not climb up to Dome C. *Gallée et al. (2014b)* present a detailed analysis of the temporal series and vertical profiles of the kinetic energy budget.

5.2 December, 11-12th, 2009

The present simulations are performed on a flat single-grid domain, so that other mechanisms than katabatic flows, are at stake to generate the simulated low level jet. Hodographs from observed and simulated

wind vectors are drawn in Figure 17. At each level the wind is turning anti-clockwise. A turn is completed in approximately 11-12 h. As we go up along the tower or in the model, the oscillation starts sooner and stops later, so that there is time to initiate a second turn. Going back to Figure 11, we see that above 20 m in the observations, and above 100 m in the simulation, two maxima are observed shifted from $11.5 \text{ h} \pm 0.15$ in simulation and $11.6 \text{ h} \pm 0.5$ in the model. This duration corresponds to the duration of one turn and to the inertial period $T_{io} = 1/f_c$, where f_c is the Coriolis parameter equal to $1.510^{-4} \text{ s}^{-1}$ at Dome C.

5.3 Inertial oscillation

These observations support the inertial oscillation (IO) mechanisms for low level jets, as theorized by *Blackadar* (1957) and revisited by *van de Wiel et al.* (2010) to account for frictional effects. The theory predicts that while at evening transition, the equilibrium between the gradient pressure force, the Coriolis force, and friction is broken, the wind starts to rotate around an equilibrium profile with the period T_{io} , (*van de Wiel et al.*, 2010) :

$$\begin{aligned} u - u_e &= (v_0 - v_e) \sin\left(\frac{2\pi}{T_{io}}t\right) + (u_0 - u_e) \cos\left(\frac{2\pi}{T_{io}}t\right) \\ v - v_e &= (v_0 - v_e) \cos\left(\frac{2\pi}{T_{io}}t\right) + (u_0 - u_e) \sin\left(\frac{2\pi}{T_{io}}t\right) \end{aligned}$$

where (u_0, v_0) and (u_e, v_e) represent the initial and equilibrium velocity components[‡]. At each height the IO is independent of the IO at other heights (*van de Wiel et al.*, 2010). Friction shuts down sooner for higher level, so that oscillation at each level are out of phase. Oscillations amplitude depend also on the height through the departure between initial and equilibrium profiles. The departure is zero near the surface where both wind speeds are zero and in the free troposphere where both wind speeds are geostrophic. In between it reaches a maximum, generally around the top of the nocturnal shear layer. This explains why we observe jet-like profile.

van de Wiel et al. (2010) found that a "reverse

[‡]. u_e corresponds the geostrophic wind in *Blackadar* (1957).

oscillation" may take place at low level during an inertial oscillation. This may contribute to the weakening of near-surface wind. Such a "clockwise oscillation" has not been observed in our case, neither on the observations nor in the simulation.

According to the theory, the amplitude of the oscillation is larger when the contrast in turbulence intensity between day and night is larger. Such contrasts are reinforced by the weaker role of the turbulent latent heat flux at Dome C, leading to a stronger diurnal cycle of the sensible heat flux. This also explain why at Dome C, jets are observed during clear sky and weak wind conditions : this conditions leads to a stronger inversion. This fact also supports that Dome C, in the summer, is an ideal site to study inertial oscillations thanks to the occurrences of both a convective boundary layer in afternoon and a strongly stable stratification at "night". This kind of jets are thus not expected on typical winter days.

6 CONCLUSION

Although the sun never disappears below the horizon, the summertime boundary layer at Dome C experiences a clear diurnal cycle. A rapid transition between a very stable boundary layer and its associated jet and a diurnal convective boundary layer is observed. This offers an ideal case in the real world to test turbulent schemes, and learn about stable regimes. This is the goal of the freshly launched GABLS4 intercomparison project (<http://www.cnrm.meteo.fr/aladin/meshtml/GABLS4/GABLS4.html>) organized by CNRM/GAME and LGGE. The present simulation does not perform as well as it should to fit observed data. The nocturnal cooling is underestimated leading to a far too deep and not stable enough inversion layer. Some more work is required in order to understand the simulation failures and improve the results. In particular, a simulation with a prescribed surface temperature may be helpful to discriminate the failures due to the turbulent scheme from those due to the surface scheme or to the coupling. Nevertheless, the comparison between the simulated night-time wind and temperature profiles with the obser-

vations do show some similarities : on both, a short live low level jet occurs just below the top of the inversion layer.

These similarities provided clues for an interpretation of the wind speed maxima seen sometimes in the middle of the observed vertical profiles. Indeed, an insight of inertial induced jets requires fine vertical and temporal resolutions in both model and observation system. On the tower, almost ten meters separates the two highest anemometers so that, the short lived jet produces some unfamiliar maxima on one or two measurement samples of the observed vertical profile. These maxima had before often been interpreted as measurement errors.

Some evidence of oscillation shows that the inertial oscillation mechanism contributes to the formation of this jet. Of course, there may also be other underlying processes feeding the jet. Studies with three dimensional models constrained by good quality large scale atmospheric forcing and able to reproduce the fine scale turbulence as done in *Gallée et al.* (2014b) are necessary for a comprehensive understanding of the underlying mechanisms responsible for the low level jet.

Inertial induced low level jets at Dome C, may appear anecdotal. Yet, in other latitudes, low level jets may interfere with other processes like the dispersion of pollutants in stable cases or birds migrations. Inertial induced jet and the induced shear-driven turbulence may usefully be considered to adjust the height of wind farms, design their turbines, program the flight of a drone and train carrier-pigeon. The good behaviour of the *Gallée et al.* (2014b) model MAR in simulating boundary layer processes at Dome C is not stranger to its good behaviour over Belgium (*Doutreloup et al.*, 2014). We argue that the dataset of the full-scale laboratory Dome C could be useful for every one interested in low level jets or other stable boundary layers related features. Besides, anyone trying to design a simulation for low level jet by inertial oscillations, whether he is from the meteorological or climate communities or not, is encouraged to take part in the GABLS4 intercomparison.

	$\frac{\partial\theta}{\partial z}$	e	K_h	$\overline{w'\theta'}$
	Km ⁻¹	m ² s ⁻²	m ² s ⁻¹	Kms ⁻¹
simulation ▲	0.09	0.04	0.10	-0.01
obs and EC calculations ◆	0.45	0.05	0.001	-0.0005
analytic 1 ▼	0.09	0.04	0.13	-0.012
analytic 2 ▼	0.45	0.04	0.06	-0.03

TABLE 2 – Values of the vertical gradient of temperature, turbulent kinetic energy and eddy diffusivity coefficients at 0LT, at 7 m. The gradients are computed from the two closest measurement or model points above and below 7 m.

Line 1 : simulated values; line 2 : values deduced from observation and EC methods; line 3 : K_h is computed from equation (4) and simulated values; line 4 : K_h is computed from equation (4) and observed values.

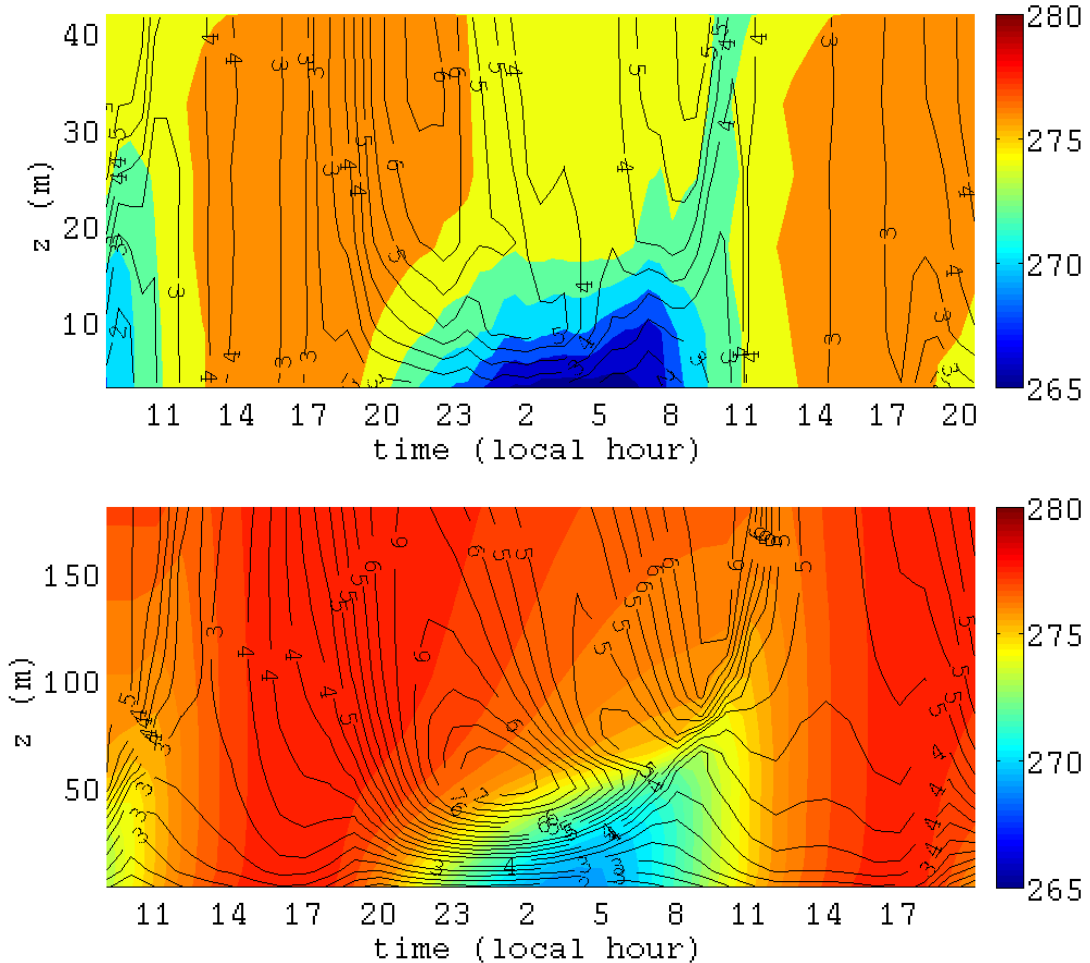


FIGURE 8 – Potential temperature and wind speed isocontours from tower observations (top) and in the 180 first meters of the simulation (bottom). Potential temperature, calculated with a reference level at 1013 hPa, ranges so "high" above 0 °C due to the elevated altitude of Dome C and the associated low pressure (~ 650 hPa). Corresponding absolute temperature is of about -30 °C.

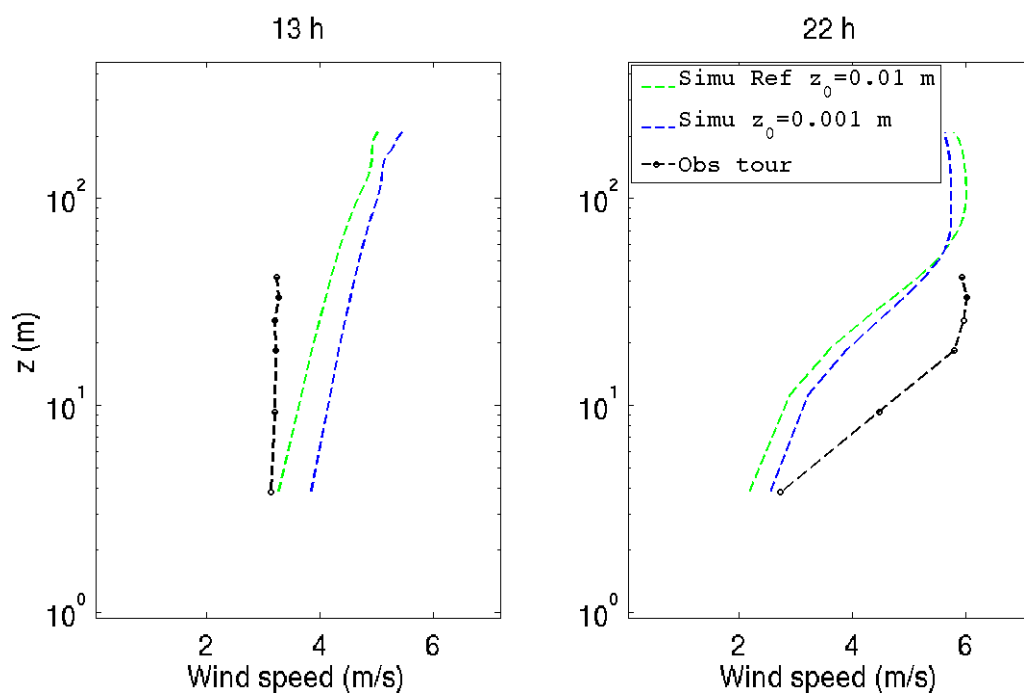


FIGURE 9 – Wind velocity profiles at 1 pm and 10 pm. Tower observations in black are compared with the control simulation (in green) and a simulation Simu2 with a lower value of the rugosity length.

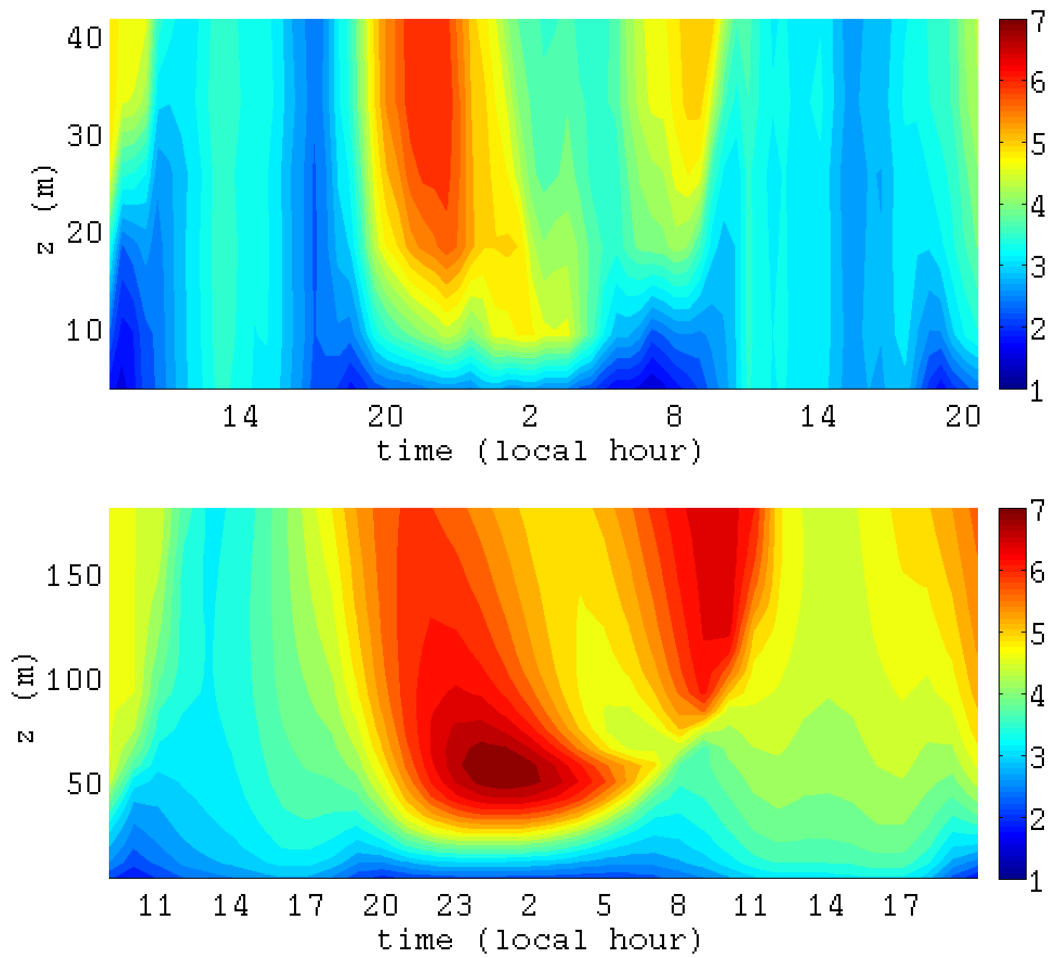


FIGURE 10 – Wind speed isocontours from tower observations (top) and in the 180 first meters of the simulation (bottom).

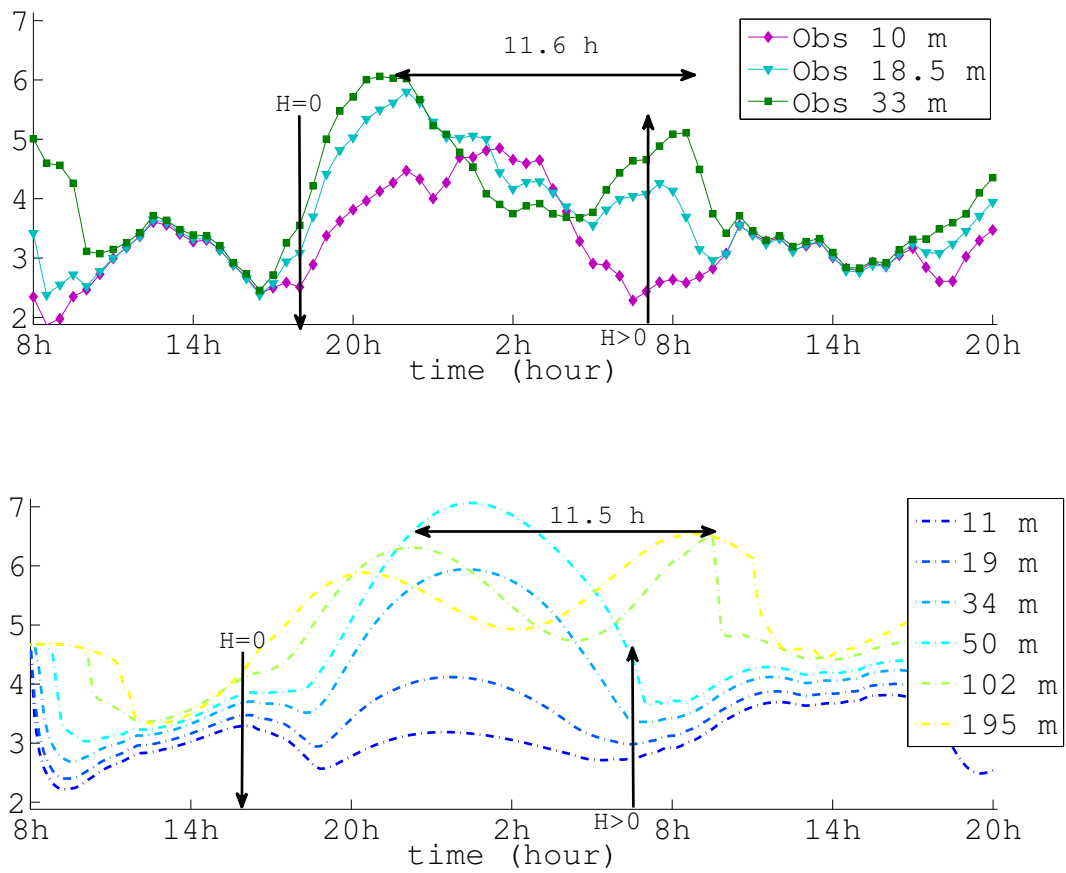


FIGURE 11 – Horizontal wind speed in ms^{-1} ; temporal series at different levels in the observations (top) and in the model (bottom).

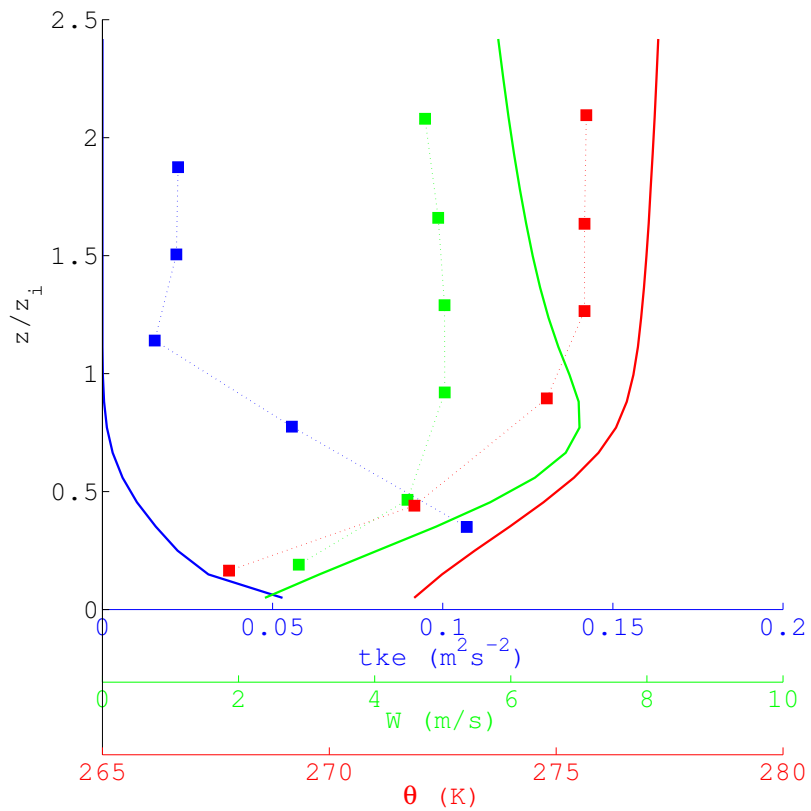


FIGURE 12 – Vertical profiles of potential temperature, wind speed and turbulent kinetic energy. Data are shown at midnight. Observational data from the tower are shown by the square; simulation results are represented by the solid line. The vertical scale is normalized with the ground-base inversion layer depth (20 m in the observational data and 60 m in the simulation).

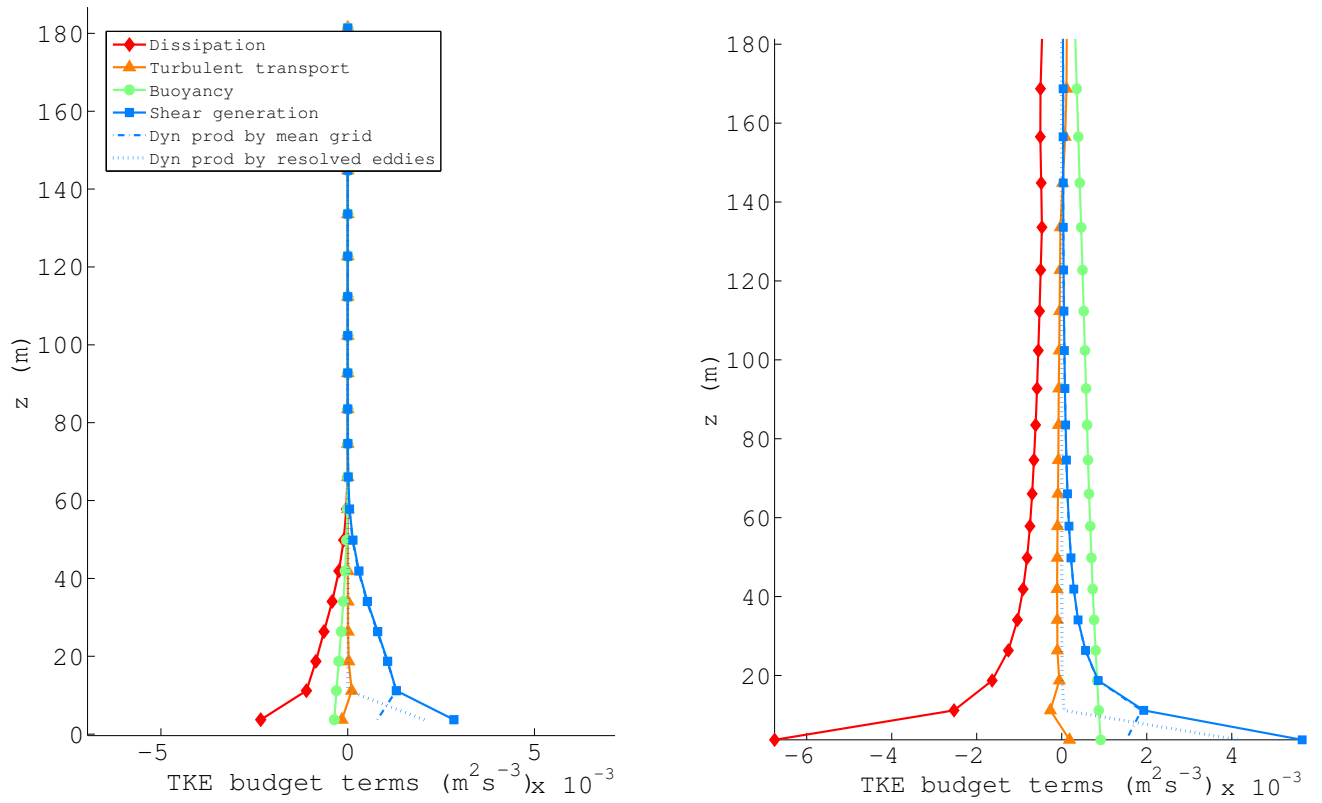


FIGURE 13 – Vertical profile of TKE budget computed from 1-hour statistics :
a. at 0 LT,
b. at 12 LT.

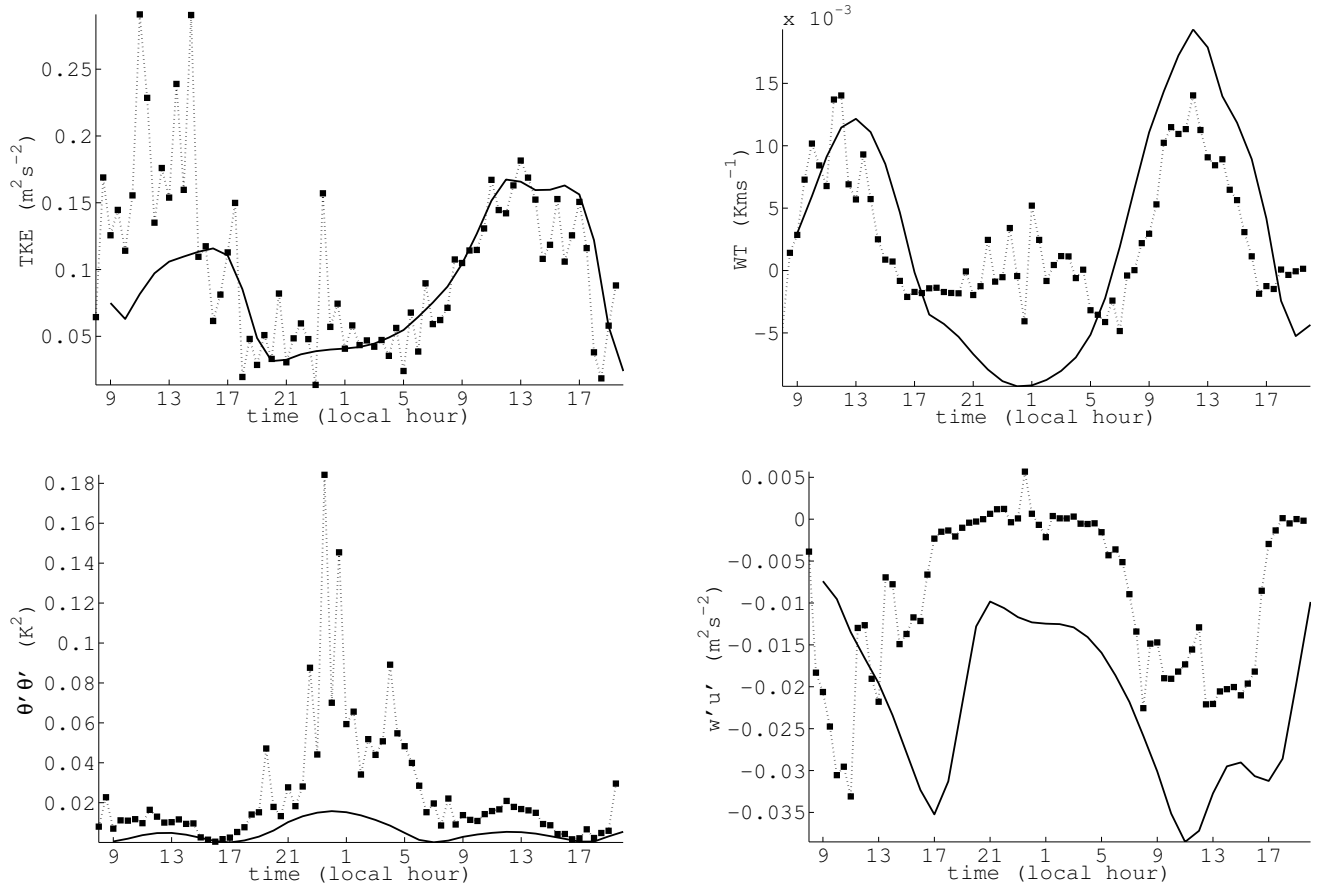


FIGURE 14 – Temporal series at 7 m, simulated (solid line) and computed from sonic anemometers (square) :

- a. Turbulent kinetic energy e (m^2s^{-2}),
- b. $\overline{w'\theta'}$ (Ks^{-1}),
- c. $\overline{\theta'^2}$ (K^2),
- b. $\overline{w'v'}$ (m^2s^{-2}).

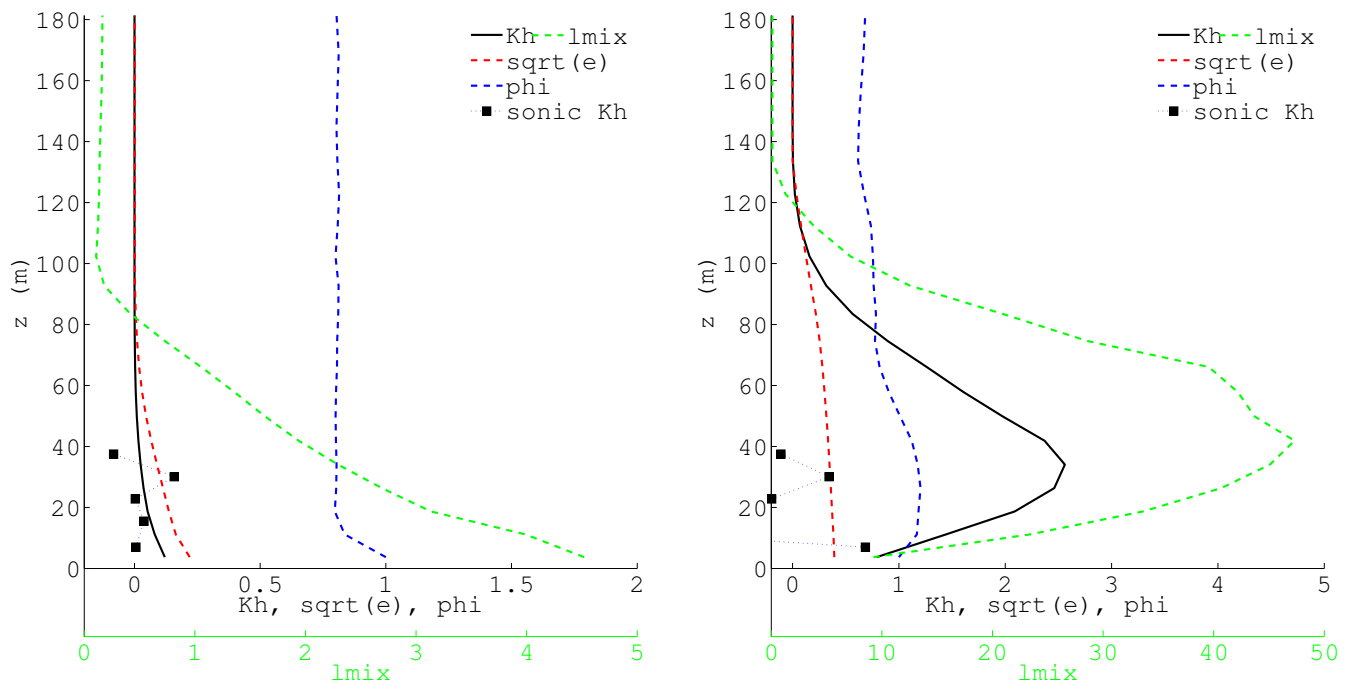


FIGURE 15 – Vertical profile the eddy diffusivity coefficient K_h in m^2s^{-1} (black solid line). The green dashed line represents the mixing length l in m, the blue dashed line, the stability function ϕ and the red dashed line the square out of the TKE (\sqrt{e}) in ms^{-1} . The black squares stand for the eddy diffusivity coefficients K_h computed from sonic data. Note that l has its own horizontal scale.

a. at 0 LT,
b. at 12 LT.

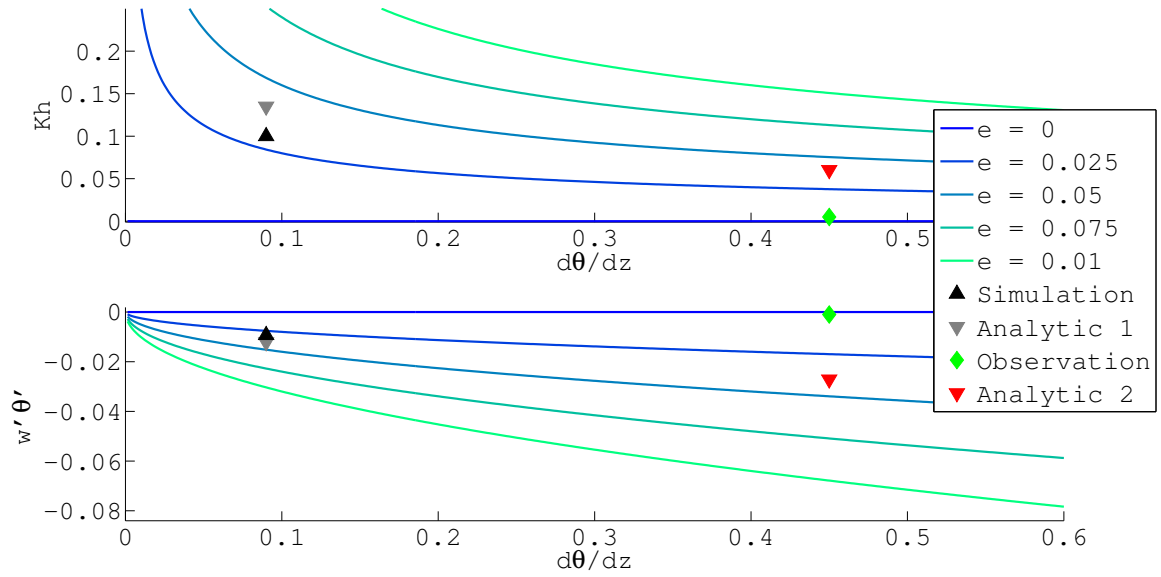


FIGURE 16 – a. Curves of the eddy diffusivity coefficient K_h in equation (4), as a function of the local vertical gradient $\frac{\partial \bar{\theta}}{\partial z}$, for different values of TKE (e in m^2s^{-2}).
 b. Curves of the heat flux $\overline{w'\theta'} = -K_h \cdot \frac{\partial \bar{\theta}}{\partial z}$, as a function of the local vertical gradient $\frac{\partial \bar{\theta}}{\partial z}$, for different values of TKE.
 The four superposed characteristic points are described in Table 2.

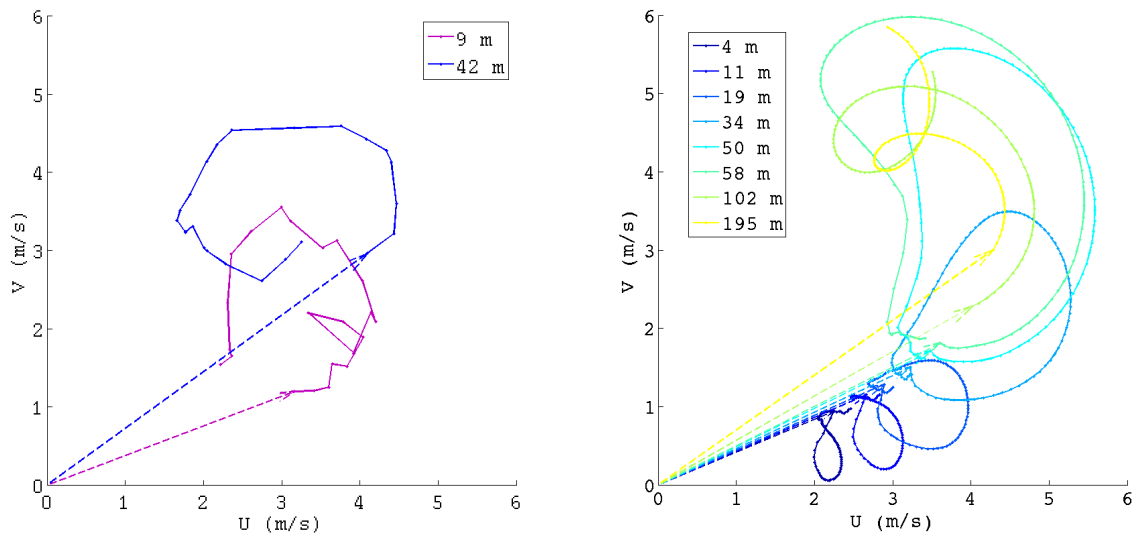


FIGURE 17 – Hodographs for different vertical levels in observation (left) and in the model (right). Dashed and coloured arrays stand for the evening velocity vectors (7 pm). Grey dashed vectors represent the maximum wind speed for each level. The observed wind is plotted from 7 pm to 6 am; the simulated wind is plotted from 7 pm to 9 am.

Références

- Argentini, S., A. Viola, A. M. Sempreviva, and I. Petenko (2005), Summer boundary-layer height at the plateau site of Dome C, Antarctica, *Boundary-Layer Meteorology*, 115, 409–422.
- Argentini, S., I. Petenko, A. Viola, G. Mastrantonio, I. Pietroni, G. Casasanta, E. Aristidi, and C. Genthon (2014), The surface layer observed by a high-resolution sodar at Dome C, Antarctica, *Annals of Geophysics*, 56(5).
- Bazile, E., O. Traullé, H. Barral, T. Vihma, A. Holtslag, and G. Svensson (2013), GABLS4 : an intercomparison case for 1D models to study the stable boundary layer at Dome C on the Antarctic plateau, in *13th EMS Annual Meeting*, Reading UK.
- Bazile, E., O. Traullé, H. Barral, V. Guillard, A. A. M. Holtslag, G. Svensson, and T. Vihma (2014), GABLS4 : An intercomparison case to study the stable boundary layer with surface interactions on the Antarctic plateau, in *AMS : 21st Symposium on Boundary Layers and Turbulence*, Leeds, UK.
- Blackadar (1957), Boundary layer wind maxima and their significance for the growth of nocturnal inversions., *Bulletin of American Meteorological Society*, 38, 283–290.
- Bougeault, P., and P. Lacarrère (1989), Parametrization of orography-induced turbulence in a mesoscale model, *Monthly Weather Review*, 117.
- Conangla, L., and J. Cuxart (2006), On the turbulence in the upper part of the low-level jet : An experimental and numerical study, *Boundary-Layer Meteorology*, 118(2), 379–400.
- Cuxart, J., and M. Jiménez (2007), Mixing processes in a nocturnal low-level jet : An LES study, *Journal of the atmospheric sciences*, 64(5), 1666–1679.
- Cuxart, J., P. Bougeault, and J.-L. Redelsperger (2000), A turbulence scheme allowing for mesoscale and large-eddy simulations, *Quarterly Journal of the Royal Meteorological Society*, 126(562), 1–30.
- Doutreloup, S., X. Fettweis, J. Beaumet, and M. Erpicum (2014), Comparaison entre le profil vertical de la vitesse du vent observé dans les basses couches de la troposphère et celui simulé par le modèle WRF en Belgique, in *XXVIIe Colloque de l'Association Internationale de Climatologie*, Dijon, France.
- Gallée, H., et al. (2014a), Characterization of the boundary layer at Dome C during OPALE, submitted.
- Gallée, H., H. Barral, E. Vignon, and C. Genthon (2014b), A case study of a low level jet during OPALE, submitted.
- Genthon, C., M. Town, D. Six, V. Favier, S. Argentini, and P. A. (2010), Meteorological atmospheric boundary layer measurements and ECMWF, analyses during summer at Dome C, Antarctica, *Journal of Geophysical Research : Atmospheres*, 115, doi : 10.1029/2009JD012741.
- Genthon, C., D. Six, V. Favier, M. Lazzara, and L. Keller (2011), Atmospheric temperature measurement biases on the Antarctic plateau, *Journal of Atmospheric and Oceanic Technology*, 28, 1598–1605.
- Genthon, C., D. Six, H. Gallée, P. Grigioni, and A. Pellegrini (2013), Two years of atmospheric boundary layer observations on a 45-m tower at Dome C on the Antarctic plateau, *Journal of Geophysical Research : Atmospheres*, doi :10.1002/jgrd.50128.
- Gregory, D., J.-J. Morcrette, C. Jakob, A. C. M. Beljaars, and T. Stockdale (2000), Revision of convection, radiation and cloud schemes in the ECMWF integrated forecasting system, *Quarterly Journal of the Royal Meteorological Society*, 126(566), 1685–1710.
- King, J. C., and J. Turner (1997), *Antarctic meteorology and climatology*, xi, 409 p. : pp., Cambridge University Press.

- King, J. C., S. Argentini, and P. S. Anderson (2006), Contrasts between the summertime surface energy balance and boundary layer structure at Dome C and Halley stations, Antarctica, *Journal of Geophysical Research*, *111*, doi :10.1029/2005JD006130.
- Lafore, J. P., et al. (1998), The Meso-NH atmospheric simulation system. Part I : adiabatic formulation and control simulations, *Annales Geophysicae*, *16*(1), 90–109.
- Manins, P. C., and B. L. Sawford (1979), A model of katabatic winds, *Journal of the Atmospheric Sciences*, *36*(4), 619–630.
- Masson, V., et al. (2013), The SURFEXv7.2 land and ocean surface platform for coupled or offline simulation of earth surface variables and fluxes, *Geoscientific Model Development*, *6*(4), 929–960.
- Parish, T. R., and D. H. Bromwich (2007), Reexamination of the near-surface airflow over the Antarctic continent and implications on atmospheric circulations at high southern latitudes, *Monthly Weather Review*, *135*(5), 1961–1973.
- Pergaud, J., V. Masson, S. Malardel, and F. Couvreux (2009), A parameterization of dry thermals and shallow cumuli for mesoscale numerical weather prediction, *Boundary-Layer Meteorology*, *132*(1), 83–106.
- Phillpot, H. R., and J. W. Zillman (1970), The surface temperature inversion over the Antarctic continent, *Journal of Geophysical Research*, *75*(21), 4161–4169.
- Pinty, J.-P., and P. Jabouille (1998), A mixed-phase cloud parameterization for use in mesoscale non-hydrostatic model : simulations of a squall line and of orographic precipitations., in *Proceedings Conference of Cloud Physics*.
- Rabier, F., et al. (2010), The Concordiasi project in Antarctica, *Bulletin of the American Meteorological Society*, *91*(1), 69–86.
- Redelsperger, J., and G. Sommeria (1982), Méthode de représentation de la turbulence associée aux précipitations dans un modèle tri-dimensionnel de convection nuageuse, *Boundary-Layer Meteorology*, *24*(2), 231–252.
- Ricaud, P., et al. (2011), Summer to winter diurnal variabilities of temperature and water vapour in the lowermost troposphere as observed by HAMSTRAD over Dome C, Antarctica, *Boundary-Layer Meteorology*, *143*(1), 1–33.
- Seity, Y., P. Brousseau, S. Malardel, G. Hello, P. Bénard, F. Bouttier, C. Lac, and V. Masson (2010), The AROME-France convective-scale operational model, *Monthly Weather Review*, *139*(3), 976–991.
- van de Wiel, B., A. F. Moene, G. J. Steeneveld, P. Baas, F. C. Bosveld, and A. A. M. Holtslag (2010), A conceptual view on inertial oscillations and nocturnal low-level jets, *Journal of the Atmospheric Sciences*, *67*(8), 2679–2689.
- Vignon, E. (2014), Couches limites atmosphériques extrêmes en Antarctique : le cas GABLS4, Master’s thesis, Paris 6 University.